Journal of Nanobiotechnology

RESEARCH

Open Access

A bioinspired supramolecular nanoprodrug for precision therapy of B-cell non-Hodgkin's lymphoma

Qixiong Zhang[1*], Yuhan Tian[2], Yanrui Yang[2], Qiuying Huang[2], Haibo Feng[3], Rui Zeng[2] and Shanshan Li[2*]

Abstract

Fludarabine (FA) is still considered as a first-line chemotherapy drug for hematological tumors related to B lymphocytes. However, it is worth noting that the non-specific distribution and non-different cytotoxicity of FA may lead to irreversible consequences such as central nervous system damage such as blindness, coma, and even death. Therefore, it is very important to develop a system to targeting delivery FA. In preliminary studies, it was found that B lymphoma cells would specific highly expressing the sialic acid-binding immunoglobulin-like lectin 2 (known as CD22). Inspired by the specific recognition of sialic acid residues and CD22, we have developed a supramolecular prodrug based on polysialic acid, an endogenous biomacromolecule, achieving targeted-therapy of B-cell non-Hodgkin's lymphoma (B-NHL). Specifically, the prepared hydrophobic reactive oxygen species-responsive FA dimeric prodrug (F_2A) interacts with the TPSA, which polysialic acid were modified by the thymidine derivatives, through non-covalent intermolecular interactions similar to "Watson–Crick" base pairing, resulting in the formation of nanoscale supramolecular prodrug (F@TPSA). Cell experiments have confirmed that F@TPSA can be endocytosed by $CD22^+$ B lymphoma cells including Raji and Ramos cells, and there is a significant difference of endocytosis in other leukocytes. Furthermore, in B-NHL mouse model, compared with FA, F@TPSA is determined to have a stronger tumor targeting and inhibitory effect. More importantly, the distribution of F@TPSA in vivo tends to be enriched in lymphoma tissue rather than nonspecific, thus reducing the leukopenia of FA. The targeted delivery system based on PSA provides a new prodrug modification strategy for targeted treatment of B-NHL.

Keywords Fludarabine, Supramolecular nanoprodrug, Polysialic acid, B-cell lymphoma, Watson–Crick base pairing

*Correspondence:
Qixiong Zhang
qixiongzhang@outlook.com; zhangqixiong@uestc.edu.cn
Shanshan Li
sslscu2009@163.com
Full list of author information is available at the end of the article

Graphical abstract

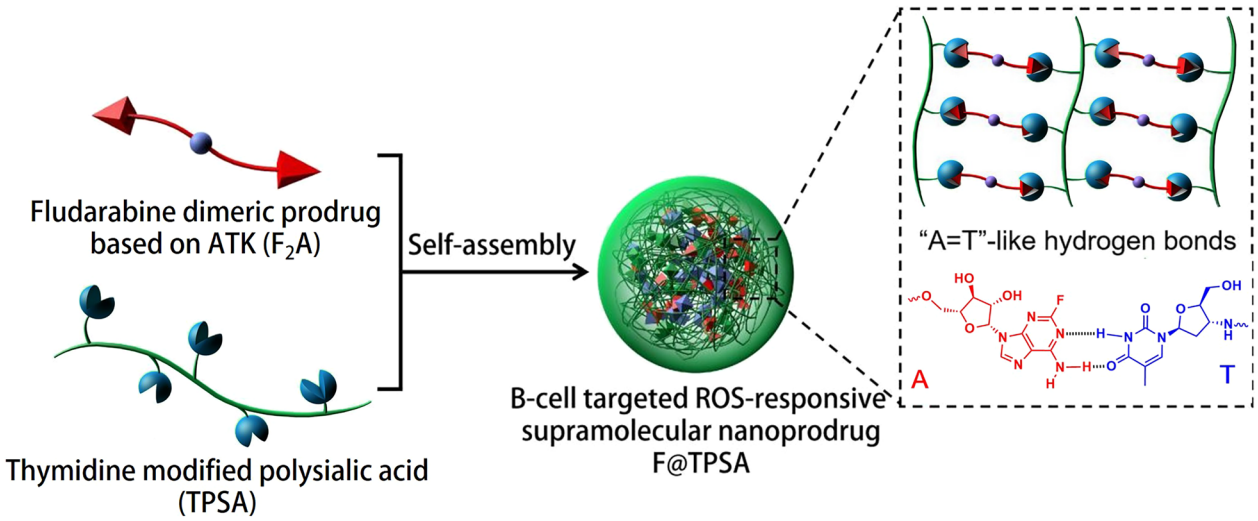

Introduction

B-cell non-Hodgkin's lymphoma (B-NHL) is a common malignancy, accounting for 70–85% of NHL [1]. Due to the distribution of the lymphatic system, surgical treatment is not feasible. Although immunotherapy based on antibodies or CAR has recently brought new hope for lymphoma patients [2–4], chemotherapy drugs are still the first choice in clinical treatment due to the high cost of antibody therapy and the different sensitivity of patients [5]. The adenine nucleoside analogue fludarabine (FA) is considered as a first-line chemotherapy agent in the treatment of B-NHL, and its main mechanism of action is to promote apoptosis by inhibiting DNA polymerase and RNA reductase [6, 7]. FA combined with cyclophosphamide or rituximab for B-NHL treatment has been widely used in clinical practice [8]. However, the non-specific distribution and undifferentiated cytotoxicity of systemic FA administration will not only cause severe leukopenia and affect subsequent bone marrow transplantation, but also lead to irreversible consequences such as blindness, coma and other central nervous system damage or even death. Through clinical and literature research, except for continuous monitoring of hematological and non-hematological toxicity, there is no clear plan to avoid the above toxic side effects of FA [9].

Recently, drug delivery systems, especially targeted drug delivery systems, have provided a favorable platform to circumvent these shortcomings [10, 11]. It is well known that B-NHL consists of five types, which can be converted to each other, so there is an urgent need for a universal and accurate B-NHL-specific targeted drug delivery systems [12]. Previous studies have found that sialic acid binding immunoglobulin-like lectin 2 (Siglec-2, also known as CD22) is a marker of B cell expression, especially malignant B cells [13]. Such a restrictive expression and endocytosis make CD22 a promising general therapeutic target for B-NHL [14]. For example, CD22-specific antibodies and antibody–drug conjugations (ADC) have shown clinical efficacy in the treatment of invasive and follicular non-Hodgkin's lymphoma, acute lymphoblastic leukemia, and diffuse large B-cell lymphoma [15]. However, due to the strong affinity of artificially designed monoclonal antibodies, these antibodies/ADC often fail to distinguish between healthy and malignant B cells, resulting in serious side effects such as low blood counts, systemic cytotoxic effects, and venous occlusive disease [16]. Fry and colleagues recently reported that an anti-CD22 CAR-T induced a good rate of cellular response in patients with acute lymphoblastic leukemia. Nevertheless, CAR-T therapy faces the same dilemma of tumor off-target toxicity [17, 18].

Fortunately, on the one hand, polysialic acid (PSA) is non-immunogenic, has good biocompatibility and biodegradability [19], and is considered to replace polyethylene glycol (PEG) to improve the stability of protein or peptide drugs in the body [20]. After polysialylation, proteins such as catalase, asparaginase, natto kinase, insulin, superoxide dismutase and antibody can prolong their circulation time in the body while maintaining the stability of biological activity [21–26]. On the other hand, PSA or oligosaccharides containing sialic acid are natural ligands of CD22 [27]. Recently, researchers have genetically modified NK cells to express Sialyl Lewis X

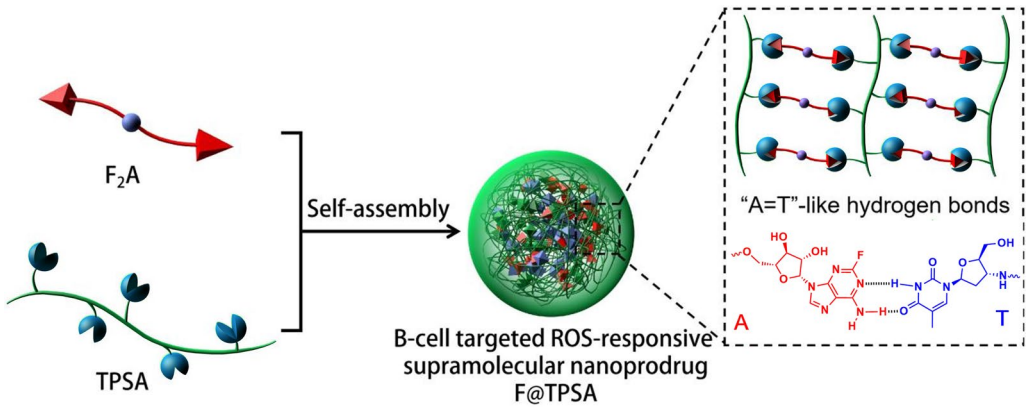

Fig. 1 The novel ROS responsive linker-based dimeric fludarabine prodrug (F_2A) and thymidine derivatives-modified polysialic acid (TPSA) exhibit an interaction similar to "Watson–Crick base pairing" in aqueous solution. The supramolecular nanoprodrug (F@TPSA) is formed by hydrogen bond and hydrophobic interaction

functionalized oligosaccharides as ligands for CD22, and found that these modified NK cells can accurately target B-cell lymphoma [28]. Our research group has also developed a PSA modified PLGA nanoparticles loaded with MTO, which can effectively enrich B lymphoma tissue through CD22 mediated selective endocytosis and fully induce immunogenic cell death (ICD) and subsequent anti-tumor immune response [29]. These reports all demonstrate that PSA is a material with potential for targeted therapy of B-NHL.

However, we also found that these studies used PSA as a surface-engineered accessory rather than the main skeleton, and the targeting efficiency of the system depends on the degree of PSA modification. At the same time, drug delivery systems based on traditional physical encapsulation methods (represented by PLGA) are difficult to achieve high drug loading, and have shortcomings such as extra targeted functionalization and unresponsive release performance.

It is worth noting that the prodrug based delivery systems developed in recent years have significant advantages in terms of drug response release, drug load, and reduced excipient use [30]. Therefore, as shown in Fig. 1, FA was transformed into a hydrophobic dimeric prodrug (F_2A) based on aromatic thioketal (ATK), a ROS responsive linker previously developed by our laboratory. At the same time, inspired by "Watson–Crick" base pairing, a large number of thymine nucleoside analogues (Thy-NH_2) were grafted on PSA to form water-soluble B-NHL-targeted biomaterials, namely TPSA. In aqueous solution, abundant hydrogen bonds like "A = T" are formed between F_2A and TPSA. In other words, F_2A as a small molecule crosslinking agent induces strong crosslinking effects between TPSAs. Finally, due to appropriate amphiphilicity, F_2A and TPSA co-self-assemble into hydrogen bonding based supramolecular nanoprodrug (F@TPSA). Further, a series of in vitro and in vivo experiments were conducted to investigate the responsive drug release ability and the targeted therapy effect of F@TPSA on B-NHL.

Materials and methods

Materials, cell culture and animals

Polysialic acid (PSA, Mw = 50 kDa) was purchased from HIGRAND Biotech Co., Ltd. (China). Poly(lactic-*co*-glycolic acid) (PLGA, 75:25) was obtained from Sigma-Aldrich (USA, Cat#430471). 1-(3-Dimethylaminopropyl)-3-ethylcarbodiimide Hydrochloride (EDCI, Cat#D1601) and *N*-Hydroxysuccinimide (NHS, Cat#H0623) were purchased from TCI (Japan). Fludarabine (FA, Cat#1025979) was obtained from Leyan (Shanghai, China). *N,N′*-Carbonyldiimidazole (CDI, Cat#C109315) and 3′-Amino-2′,3′-dideoxythymidine (Thy-NH_2, Cat#A122927) were purchased from Aladdin (China). The aromatic thioketal (ATK, refer as 4,4′-((9H-fluorene-9,9-diyl)bis(sulfanediyl))dibutyric acid) was prepared by our lab [31, 32].

Dulbecco's Modified Eagle's medium (DMEM), fetal bovine serum (FBS), and trypsin for cell culture were purchased from Gibco (USA). Purified anti-human CD22 antibody (Cat#382701), FITC-labeled anti-human CD22 antibody (Cat#363508), Apotracker™ Green (Cat#427403) and purified anti-human Ki-67 antibody (Cat#350502) were purchased from Biolegend (USA). Matrix-Gel™ Basement Membrane Matrix (Cat#C0383). Cell Proliferation and Cytotoxicity Assay Kit based on MTT (Cat#C0009S) was purchased from Beyotime Biotechnology Co. Ltd. (China). All the other reagents are commercially available and used as received.

Female CB17 SCID mice (6–8 weeks) were provided by the Charles River Co. Ltd. (China). All experimental procedures were approved and supervised by the Institutional Animal Care and Use Committee of Sichuan Provincial People's Hospital.

Synthesis and characterization of dimeric prodrug of fludarabine (F_2A)

Based on the ROS-responsive linker (ATK) developed by our lab [31, 33], dimeric prodrug (F_2A) was synthesized. Briefly, ATK (600 mg, 1.5 mmol) and CDI (1220 mg, 7.5 mmol) were dissolved in anhydrous DCM and the solution was continuously stirred at RT for 60 min. Add 10 mL DCM to the solution and transfer to the separator funnel, wash three times with 30 mL deionized water. The organic phase was further washed with saturated NaCl solution, dried with anhydrous Na_2SO_4, and concentrated by vacuum spin evaporation to obtain CDI-activated ATK (ATK-CDI). Subsequently, the dimeric prodrug F_2A was obtained by coupling FA to ATK-CDI. Specifically, FA (710 mg, 2.5 mmol), TEA (100 μL) and ATK-CDI (753 mg, 1.5 mmol) were dissolved in 8 mL anhydrous DMF under nitrogen protection and stirred overnight at RT. A large amount of cold anhydrous ether was added to the mixed solution to produce white precipitate, which was centrifuged and dried to obtain the final product F_2A (987 mg, yield 84.3%). The structures of ATK-CDI and F_2A were confirmed by ^{1}H NMR and ESI–MS.

The ROS-responsiveness of F_2A

The high performance liquid chromatography (HPLC) was applied to analyze the composition of F_2A samples incubated in different media. Briefly, 100 μL of F_2A methanol solution (5 mg/mL) was uniformly mixed with 1 mL of PBS or H_2O_2 solution (10 mM) by vortex, and then incubated under sustaining oscillation at 37 °C. At predetermined time points, mixture was withdrawn and detected with HPLC using mixture of methanol/water (75:25, v/v) as mobile phase, to measure ROS-induced degradation of F_2A.

Synthesis and characterization of thymidine derivative-grafted polysialic acid conjugate (TPSA)

PSA (100 mg, 0.34 mmol) and EDCI (260 mg, 1.36 mmol) were dissolved in 10 mL deionized water. After stirring for 30 min at RT, NHS (78 mg, 0.68 mmol) was added for further activation for 30 min. The Thy-NH_2 (164 mg, 0.68 mmol) was added and react for 20 h. The reaction solution was added dropwise into a large amount of acetone, centrifuged at 4000 rpm for 5 min to collect the white precipitate. Washed with acetone for 3 times and dried to obtain the final product TPSA (115 mg, yield 65.8%). The structure of TPSA was characterized and calculated by ^{1}H NMR.

Preparation and characterization of supramolecular nanoprodrug (F@TPSA)

The supramolecular nanoprodrug F@TPSA was prepared by the crosslinking of F_2A with TPSA following a simulative "high temperature denaturation and low-temperature annealing procedure". Briefly, 200 μL of F_2A methanol solution (25 mg/mL) was slowly injected into 10 mL of TPSA aqueous solution (0.5 mg/mL). The above solution was continuously ultrasonicated at 37 °C for another 30 min. Then, the mixture temperature increased to 70 °C maintaining for 10 min, followed by cooling to 37 °C and maintaining for 30 min under vigorous ultrasonication, to facilitate the formation of hydrogen bonds between adenine structures of F_2A and thymidine moieties of TPSA. To eliminate residual organic solvent, the solution was then concentrated under vacuum. Finally, using a water Millipore filter (0.45 μm), F@TPSA nanoformulation was obtained after filtration and stored at 4 °C for further study. The hydrodynamic nanoparticle diameter and zeta potential of F@TPSA were measured by a Malvern Zetasizer Nano ZS90 (Malvern Instruments, Malvern). The morphology of dried F@TPSA were investigated via transmission electron microscopy (JEM-1400, JEOL).

The formation mechanism of F@TPSA

In order to illustrate the interaction between Thy-NH_2 and FA, molecular docking simulation was carried out. Draw the molecular formulas for Thy-NH_2 and FA using ChemDraw Professional 16.0. The 2D molecular structure was stored as a 3D structure after energy minimization by Chem3D 16.0. Molecular docking was done by AutoDock4.2, with the conformational search number set to 100 and other parameters left as default. The conformation with the lowest Gibbs free energy was selected as the optimal conformation for the combination of Thy-NH_2 and FA, and the analysis of molecular docking results was completed by the visualization software Pymol 2.4.

Further, real-time mass spectrum changes of mixed solution during self-assembly was used to directly monitor the existing hydrogen bonds interaction between FA and Thy-NH_2. Briefly, appropriate amount of physical mixture of FA with Thy-NH_2 (molar ratio = 1:1) was

completely dissolved in water. At different temperatures (37 and 70 °C), the mass spectrum changes of mixed solution were detected by mass spectrometer.

Cell culture and intracellular uptake of F@TPSA

Raji cells, RAW264.7 cells and THP-1 cells were cultured in RPMI-1640 with 100 IU/mL penicillin, 100 μg/mL streptomycin, and 10% FBS. Ramos cells was cultured in DMEM (High glucose) with 100 IU/mL penicillin, 100 μg/mL streptomycin, and 10% FBS. Cells were maintained in a 5% CO_2 humidified atmosphere at 37 °C. In order to detect cell uptake by flow cytometry, Cy5 labeled F@TPSA and F@PLGA were prepared.

For competition assay for cellular uptake, 1×10^5 cells/well Raji cells were seed in 24 well plate with or without 35 mm glass-bottom cell culture dishes. After overnight incubation, cells pre-incubated with purified CD22 antibody for 2 h, and change the medium with 8 μg/mL F@TPSA for 1 h, and analyzed with Flowjo V10. A similar flow cytometry test was also performed in RAW264.7 cells. In addition, Raji cells were cultured overnight on a culture plate. Then, different concentration (0, 0.25, 0.5, 1, 2, 4, 8 μg/mL) of Cy5@F@TPSA was added into the culture medium. After incubation for 1 h, Raji cells were washed with PBS thrice. Intracellular Cy5 fluorescence intensity was measured by flow cytometry.

In vitro anti-tumor effects of F@TPSA

MTT is used to monitor the cell viability of Raji cells. Cells were planted at 1×10^5 cells/well in 96-well plates for 24 h. Subsequently, cells were treated with the medium containing Free FA or F_2A or F@TPSA at various concentrations (varying from 0, 0.0125, 0.025, 0.05, 0.1, 0.25, 0.5, 1, 2.5, 5, 10 μM [FA]) for 24 h. After the incubation, the medium was replaced with fresh medium. The MTT reagent and stop/solubilization solution were sequentially added with a 3 h interval. The formazan concentration was measured at 550 nm. The cell viability was normalized to the absorbance of PBS-treated control cells. The half inhibition concentration (IC_{50}) was calculated based on the results obtained.

Apoptosis analysis was conducted using Apotracker™ Green (also known as Apo-15 peptide) probe according to the manufacture's protocol. Briefly, Raji cells were treated with the medium containing Free FA or F_2A or F@TPSA at 1.5 μM [FA] for 24 h. Cells were washed with cold BioLegend's cell staining buffer, digested with 0.25 wt% trypsin, and collected by centrifugation. After the cells were resuspended in 100 μL of staining buffer with 5 μL of Apotracker™ Green diluted solution (1:10) at 1×10^6 cells/mL, they were vortexed gently and incubated in a dark room for 15 min. Finally, 400 μL of PBS was added for analysis by flow cytometry. The Apotracker™ Green will be registered in the FITC channel of the flow cytometer.

In vivo pharmacokinetics and biodistribution study of F@TPSA

SCID mouse were subcutaneously (s.c.) injected in the flank with Raji cells (2×10^6) in 50% Matrix-Gel™ Basement Membrane Matrix on day 0. When the tumor size reached > 100 mm^3, the mice were randomly divided into different groups.

Based on the B-NHL model, mice (n = 6) were injected with either FA or F@TPSA (100 mg/kg [FA]) through the tail vein. For pharmacokinetic investigation, within 24 h after injection, venous blood was collected for blood drug concentration analysis. Briefly, at predefined time points (0.5, 1, 1.5, 2, 4, 8, and 24 h), blood samples were collected. The whole blood samples were immediately centrifuged at 12,000*g* for 2 min to obtain plasma. Then 800 μL of ice-cold methanol was added into 200 μL of plasma to precipitate protein. After centrifugation at 12,000*g* for 2 min, the supernatant was purged with nitrogen, reconstituted with methanol, and detected by liquid chromatography with mass spectrometry.

In vivo anti-tumor effects and myelosuppressive effect of F@TPSA

Based on the B-NHL model, mice (n = 6) were given intravenous injection of saline, free FA or F@TPSA (100 mg/kg [FA]) once at day 14, 16 and 18, respectively. The tumors were measured with calipers and tumor volume was calculated using the formula: (length × $width^2$)/2. On the 40th day, the tumor tissue was collected, paraffin embedded, and sliced for H&E staining and Ki-67 immunohistochemical staining, respectively.

Leukopenia is a common side effect of FA. We evaluated the effects of different FA formulations on the leukocyte count of femur in tumor-bearing mice. In another parallel experiment, each group of mice was sacrificed after 40 days, unilateral femur was washed by PBS, and lavage fluid was collected. The number of total leukocyte was measured by hematologic counter.

Statistical analysis

Data were presented as the mean ± standard deviation (SD). Statistical analysis was assessed using One-way ANOVA test. A value of $p < 0.05$ was considered statistically significant.

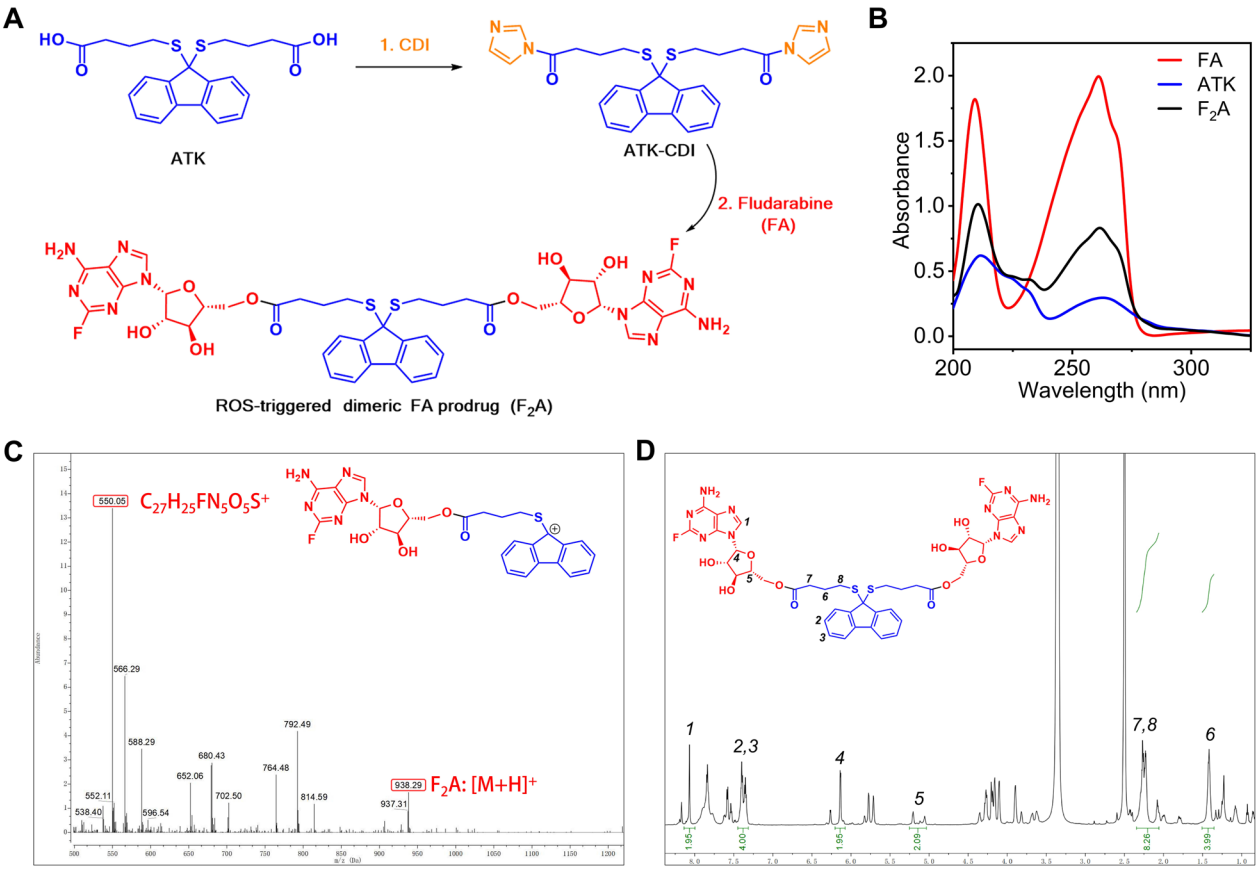

Fig. 2 Preparation and characterization of ROS-responsive dimeric prodrug of fludarabine (F_2A). **A** The synthetic route of F_2A. **B** The UV–VIS absorption spectra of FA, ATK, and F_2A. **C** The ESI–MS spectrum of F_2A. **D** The ^{1}H NMR spectra of F_2A in DMSO-d_6

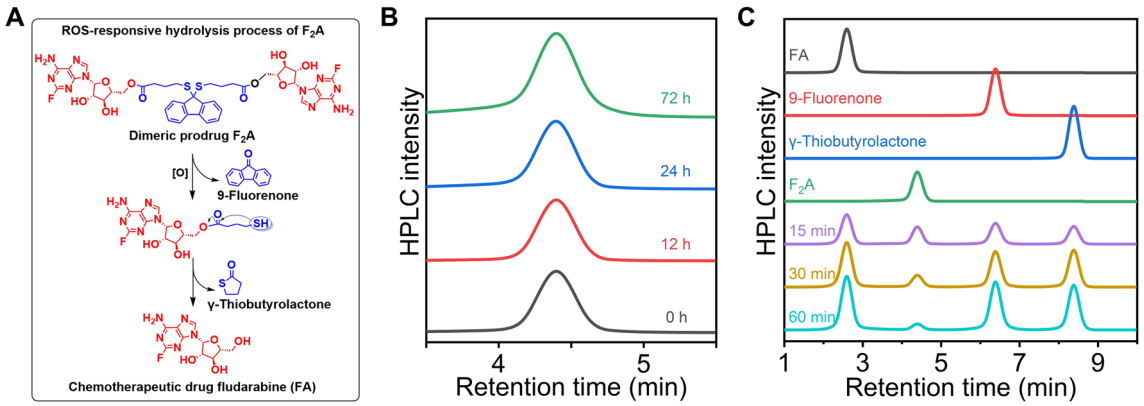

Fig. 3 The stability of F_2A in different environments. **A** ROS-responsive hydrolysis process of F_2A. **B** The HPLC analysis of F_2A incubated in PBS for different times. **C** The HPLC analysis of F_2A incubated in 1 mM H_2O_2 for different times. **B** and **C** were redrawn from Figure S3 by software OriginPro® 2018

Results and discussion

Synthesis and characterization of the dimeric prodrug F_2A

We have previously reported an aromatic thioketal (ATK), which can be used as ROS-responsive linker to prepare multiple prodrugs [31, 33] or carriers [32]. In consideration of the carboxyl and hydroxyl groups of ATK and FA, respectively, the dimeric prodrug F_2A was prepared by CDI-mediated esterification. As shown in

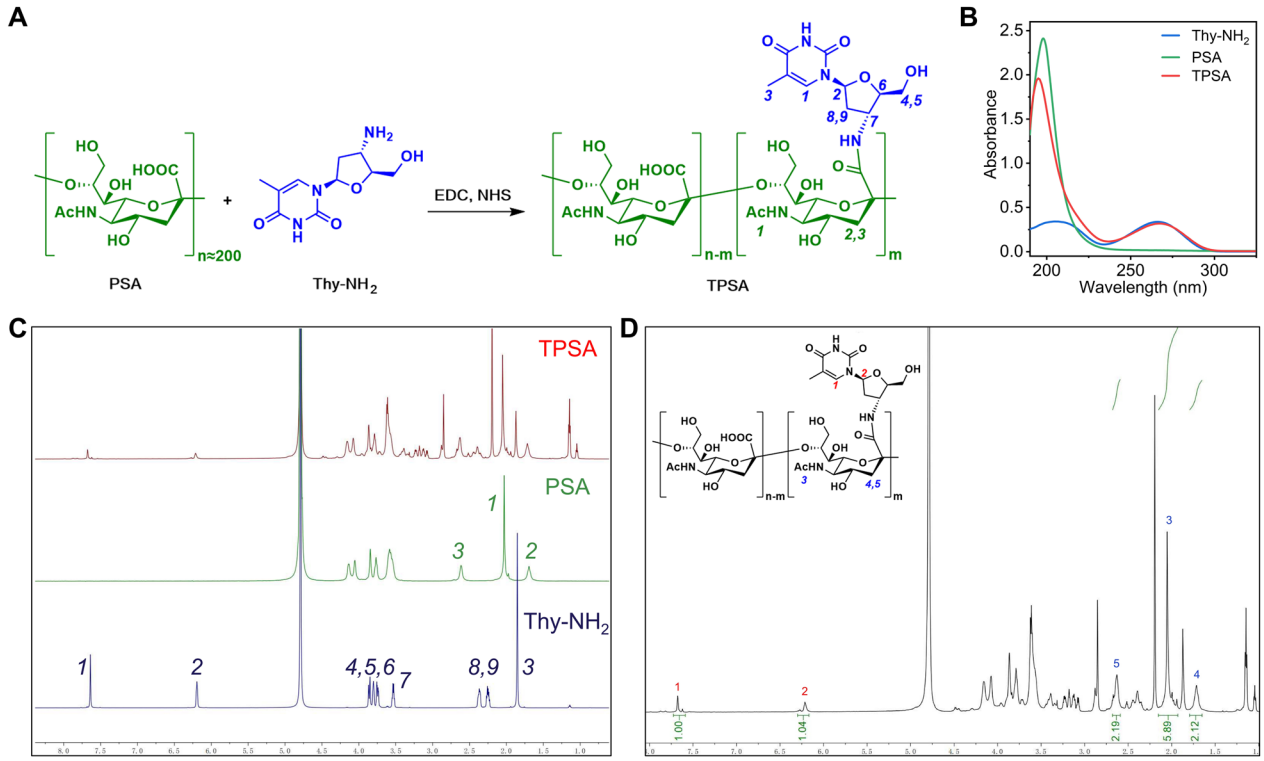

Fig. 4 Synthesis and characterization of TPSA. **A** The synthetic route of TPSA. **B** The UV–vis absorption spectra of Thy-NH_2, PSA, and TPSA. **C** The ^{1}H NMR spectra of Thy-NH_2, PSA, and TPSA in D_2O. **D** The ^{1}H NMR spectrum of TPSA in D_2O

Fig. 2A, CDI activates the two carboxyl groups of ATK to form acyl imidazole derivative ATK-CDI. The successful synthesis of ATK-CDI was confirmed by ^{1}H NMR (Figure S1) and ESI–MS spectrum (Figure S2). In the second step, the intermediate ATK-CDI undergoes a substitution reaction with FA to obtain the final product, named F_2A.

To demonstrate the exact chemical structure of F_2A, multiple characterization methods were employed. The UV–VIS spectrum shows that compared to ATK, both FA and F_2A exhibit stronger absorption at around 260 nm (Fig. 2B). This is caused by the double bond in the base group of FA, which serves as a nucleic acid analogue. This proves that FA and ATK are coupled. In order to more intuitively examine whether F_2A is a dimeric prodrug, we used ESI mass spectrometry. Figure 2C shows the ESI–MS spectrum of F_2A. ESI–MS m/z: calculated for F_2A ($C_{41}H_{42}F_2N_{10}O_{10}S_2$) $[M+H]^+$ 937.964, found 938.29; calculated for fragmentary peak of F_2A ($C_{27}H_{25}FN_5O_5S^+$) 550.585, found 550.05. These data were consistent with theoretical calculation. Moreover, it can be seen from the results that all the ^{1}H NMR peaks can be assigned to F_2A, and the ratio of protons represented by each peak is also consistent with the chemical structure of F_2A (Fig. 2D). The above characterization results all prove that the dimeric prodrug F_2A has been successfully prepared.

The ROS-responsive hydrolysis process of F_2A

According to our previous reports related to ATK [31, 33], we proposed the possible hydrolysis process and products of F_2A in ROS-containing media (Fig. 3A).

To verify this hypothesis, HPLC was used to verify the stability and response performance of the F_2A (Fig. 3B, C and Figure S3). As shown in Fig. 3B, only one substance F_2A was detected in PBS (pH 7.4) regardless of incubation for 12 h, 24 h or 72 h, which proved the excellent stability of F_2A. However, additional substances such as FA, 9-fluorenone and γ-thiobutyrolactone are detected after incubation in 1 mM H_2O_2 for only 15 min. Moreover, with the extension of incubation time, the detected concentration of F_2A gradually decreases while the concentration of other products gradually increases (Fig. 3C). After incubation for 1 h, the peak of F_2A basically disappeared, indicating that F_2A was completely degraded into other products, including the prototype drug FA. These results support our conjecture that F_2A has H_2O_2-responsive drug release properties.

Synthesis and characterization of TPSA

Aiming to introduce massive thymine structures into PSA, Thy-NH_2 was selected as thymine donor. TPSA was efficiently prepared by coupling Thy-NH_2 with PSA in

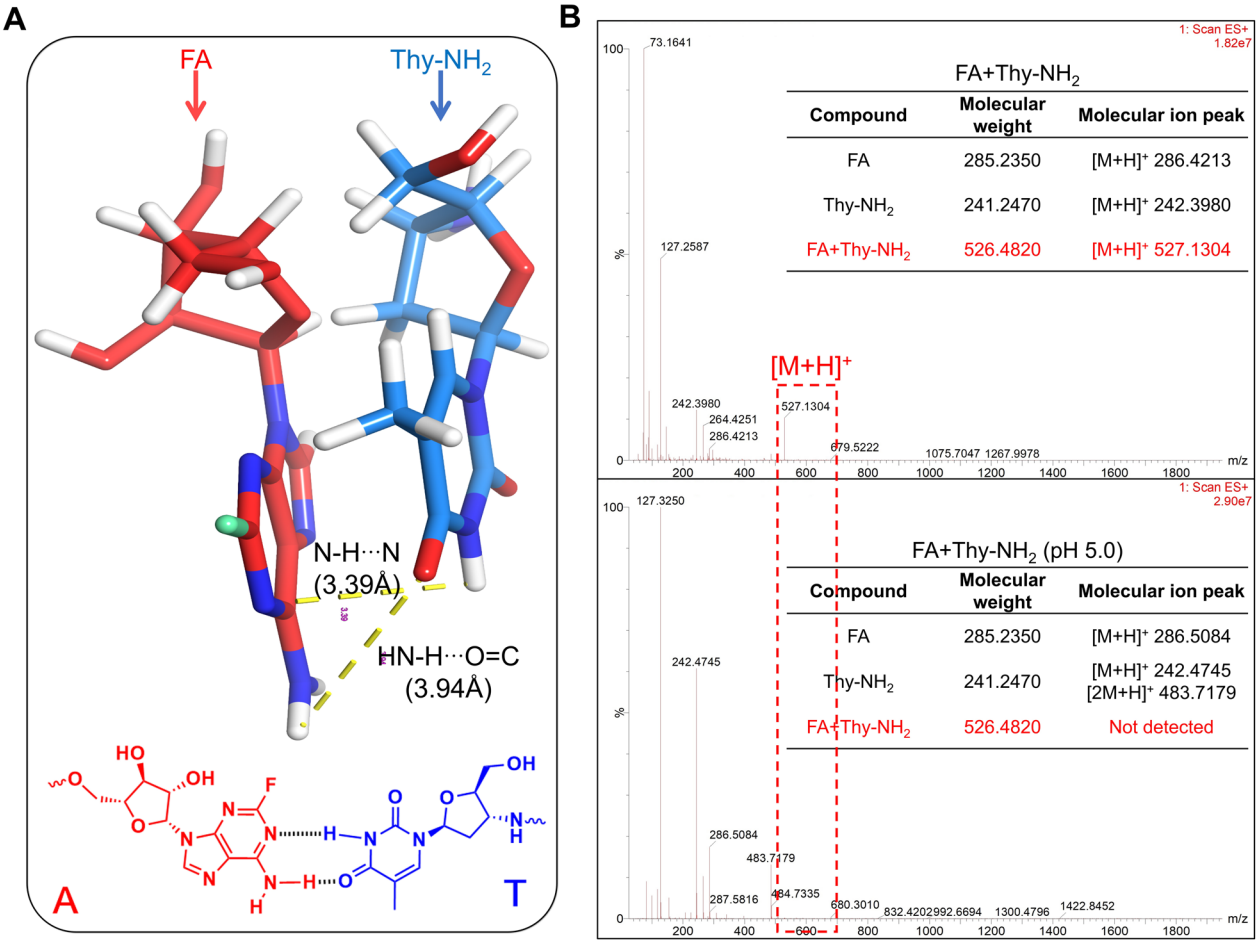

Fig. 5 Molecular dynamics simulations and mass spectrometry were used to study the interaction between FA and Thy-NH_2. **A** Molecular dynamics simulation of the interaction between FA and Thy-NH_2. **B** The MALDI-TOF MS spectra for FA, Thy-NH_2, and mixed solution of FA and Thy-NH_2

aqueous solution through EDCI/NHS mediated amidation reaction (Fig. 4A).

It can be seen from Fig. 4B that the UV–vis spectrum of PSA presents a single peak with λ_{max} of 200 nm, while TPSA is slightly blue shifted to about 190 nm. Thy-NH_2 has a relatively broad absorption peak around 210 nm and 260 nm respectively, similar to Fig. 2B, which is consistent with its characteristics as a nucleoside analogue. As expected, the TPSA sample also exhibits an absorption peak at 260 nm, indicating the presence of Thy-NH_2 groups in TPSA.

As a polysaccharide, the difference between TPSA and PSA can be detected by ^{1}H NMR. Specifically, ^{1}H NMR can reflect more detailed proton information. Figure 4C shows the comparison of ^{1}H NMR spectra of PSA, Thy-NH_2 and TPSA. Excitingly, all the characteristic peaks of PSA and Thy-NH_2 can be found in the spectrum of TPSA and are accurately assigned to each proton. It was confirmed that Thy-NH_2 was successfully grafted onto PSA. Furthermore, by performing integral analysis on the peak area of the ^{1}H NMR spectrum of TPSA (Fig. 4D), it can be concluded that there are about 50 Thy-NH_2 in every 100 SA units, that is, the grafting rate of Thy-NH_2 in TPSA is about 50%.

It is worth noting that the grafting rate of Thy-NH_2 increases with the increase of feed ratio, reaching up to about 50% (data not shown). In order to ensure that the thymidine structure can form sufficient "Watson–Crick" base pairing (A = T)-like hydrogen bond with more F_2A, and induce strong cross-linking between TPSA, the TPSA molecule with the highest grafting rate (50%) was selected for subsequent experiments.

Preparation, characterization and formation mechanism of supramolecular nanoprodrug (F@TPSA)

According to our hypothesis, the adenine structure of the dimeric prodrug can produce hydrogen bonds with the thymine structure of TPSA. In brief, simulating the process of "high temperature denaturation and low temperature annealing" can promote the formation of hydrogen

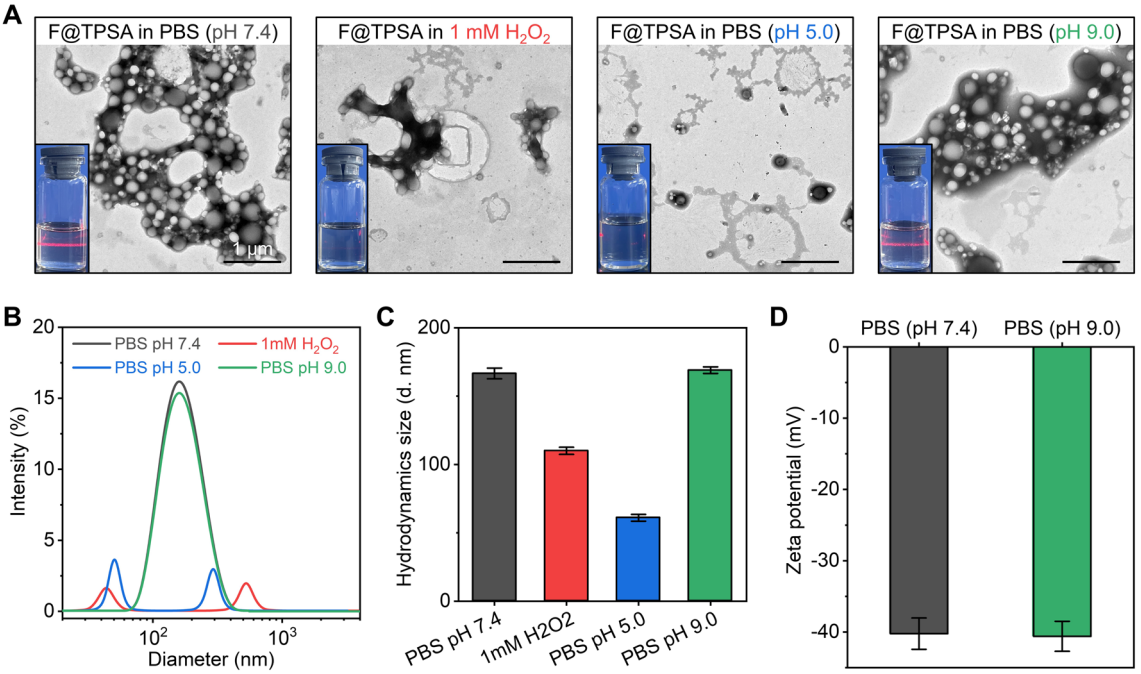

Fig. 6 Characterization of supramolecular nanoprodrug F@TPSA. **A** The digital photos and TEM photographs of F@TPSA. **B** The particle size distribution of F@TPSA in different media. **C** Comparison of the average hydrodynamic size of F@TPSA in different media. **D** The ζ-potential of F@TPSA in PBS with pH 7.4 or pH 9.0. All data are presented the mean ± SD (n = 6)

bonds. However, since the highly complex ^{1}H NMR spectra of TPSA are almost impossible to be fully identified, Molecular dynamics simulation and mass spectrometry were used to verify the hydrogen bond between FA and Thy-NH_2.

Figure 5A shows the molecular dynamics simulation results of the interaction between FA and Thy-NH_2. It can be seen that there are two hydrogen bonds similar to "A = T" between FA and Thy-NH_2, with distances of 3.39 Å and 3.94 Å respectively. In Fig. 5B, a new peak at m/z 527.1304 appeared in the mass spectrum of mixed solution of FA and Thy-NH_2 (molar ratio = 1:1) in PBS (pH 7.4), while completely disappeared at pH 5.0. This result indicated the formed hydrogen bonds would keep relatively stable under neutral, while be effectively broken under acidic environment (pH 5.0).

Inspired by Watson–Crick base pairing, supramolecular nanoprodrug F@TPSA was prepared by noncovalent cross-linking between dimeric prodrug F_2A and functional material TPSA. As shown in the digital photographs and TEM images of Fig. 6A, F@TPSA was dispersed in PBS (pH 7.4) solution to form a colloidal system with obvious Tyndall effect and regular sphericity observed, while the PBS solution of TPSA was transparent, and there was no Tyndall effect (Figure S4). Although the particle size distribution of F@TPSA measured by DLS in aqueous solution is relatively broad, it still maintains a unimodal distribution trend (Fig. 6B), and the average hydrodynamic size is about 166.6 ± 3.9 nm (Fig. 6C), which is also consistent with TEM results. Notably, F@TPSA lost the Tyndall effect when dispersed in 1 mM H_2O_2 or PBS (pH 5.0) media. The irregular sphericity was observed by TEM, while the multi-modal particle size distribution was measured by DLS. The average hydrodynamic size also decreased to 110.1 ± 2.6 nm and 61.0 ± 2.5 nm, respectively. In contrast, it seems that PBS (pH 9.0) does not cause changes in mean particle size, and particle size distribution. This suggests that F@TPSA can remain stable under physiological or alkaline conditions, while structural damage occurs in acidic or ROS environments, entirely due to the properties of hydrogen bonding and ROS-responsiveness of ATK. Meanwhile, in Fig. 6D, TPSA as the shell, provides a significant negative ζ-potential for F@TPSA, which guarantees the biocompatibility of F@TPSA in vivo. The drug loading content of F@TPSA is 32.5%.

From the above results, it can be inferred that hydrogen bonding forces dominate the formation of supramolecular nanoprodrug F@TPSA. The two terminal adenine structures of F_2A can effectively form hydrogen bonds with a large number of thymine structures in TPSA and

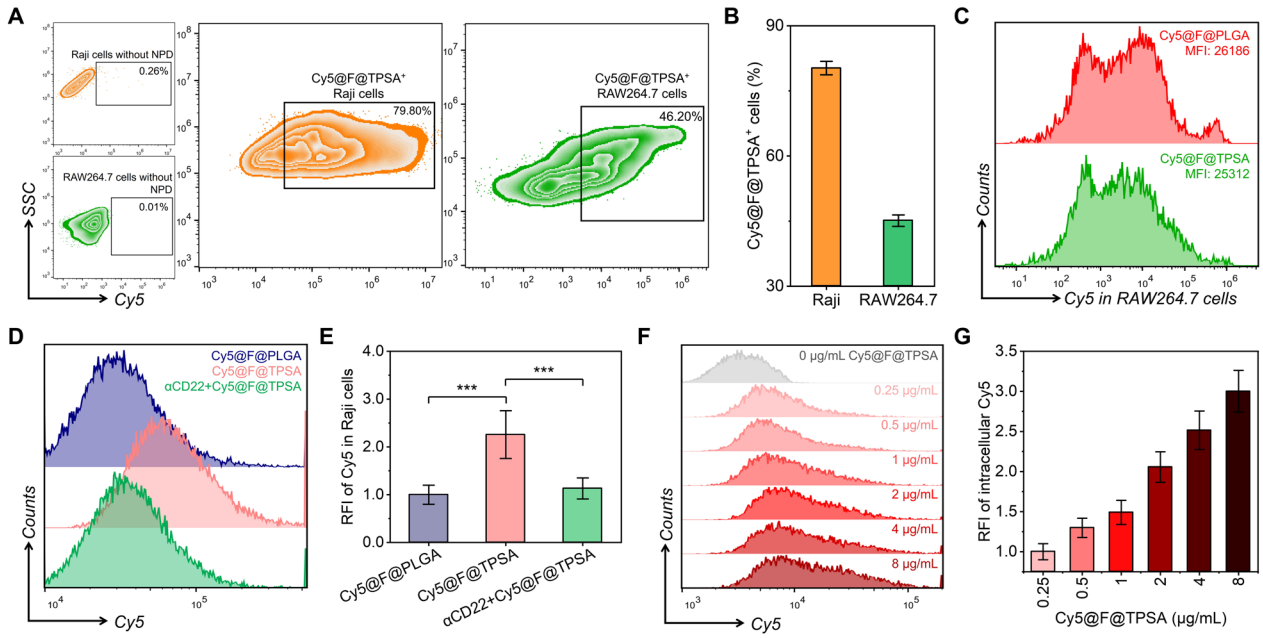

Fig. 7 Specific uptake of Cy5-labeled supramolecular prodrug of fludarabine (Cy5@F@TPSA) by B lymphoma cells in vitro. **A**, **B** Flow cytometry (**A**) and statistical analysis (**B**) of the endocytosis of Cy5@F@TPSA in Raji cells or RAW264.7 cells. **C** Comparison of endocytosis of two Cy5 labeled nanodrug (Cy5@F@TPSA and Cy5@F@PLGA) in $CD22^{-}$ RAW264.7 cells. **D**, **E** Flow cytometry (**D**) and intracellular Cy5 relative fluorescence intensity (RFI) of $CD22^{+}$ Raji cells (**E**). Cy5@F@PLGA was used as a positive control and αCD22 was a neutralizing antibody to CD22. **F**, **G** Flow cytometry (**F**) and statistics (**G**) of Cy5@F@TPSA at different concentrations (0.25, 0.5, 1, 2, 4, 8 μg/mL) after phagocytosis by Raji cells. For E, n = 6, $^{***}p < 0.001$

induce tight cross-linking between TPSAs. This supramolecular aggregate with appropriate hydrophobicity–hydrophilicity balance can further self-assemble into compact nanoparticles. The hydrophobic F_2A is located in the core, while the TPSA chain serves as a hydrophilic shell. F@TPSA has a unique drug loading method and strong cross-linking enhanced stability, which can improve the water solubility and stability of F_2A. Furthermore, due to the characteristics of hydrogen bonding and the ROS responsiveness of ATK, F@TPSA can achieve structural dissociation and drug release in acidic or oxidative stress environments. This provides a foundation for the subsequent application of F@TPSA.

F@TPSA specifically targets $CD22^{+}$ B lymphoma cell lines

The above results all prove that the supramolecular nanoprodrug F@TPSA has been successfully prepared. Next, it is necessary to confirm whether F@TPSA can be specifically uptake by CD22 positive B lymphoma cell lines. Since F@TPSA has no fluorescent properties, F@TPSA needs to be labeled. Therefore, the hydrophobic small molecule Cy5 NHS ester can be embedded with the formation of F@TPSA and is named Cy5@F@TPSA. Similarly, Cy5@F@PLGA (note: not containing PSA) was prepared as a control. Two B lymphoma cell lines (Raji cells and Ramos cells) and two other lymphoid cell lines (RAW264.7 cells and THP-1 cells) were stained using FITC-labeled CD22 antibodies. The CD22 expression levels of two B lymphoma cell lines were significantly higher than those of the other two monocyte lines measured by flow cytometry (Figure S5). Especially, the average expression level of CD22 in Raji cells is the highest, 30.3 times that of RAW264.7 cells, indicating a significant difference in CD22 expression levels between the two cell lines. Therefore, Raji cells and RAW264.7 cells were selected as the study subjects for comparison of cellular uptake.

Figure 7A shows the flow cytometry of Raji cells or RAW264.7 cells after co-incubation with Cy5@F@TPSA. However, as can be seen from Fig. 7B, the proportion of Cy5@F@TPSA positive Raji cells reached 80.26 ± 1.55%, which was significantly different from 45.11 ± 1.32% positive rate in RAW264.7 cells. This suggests that F@TPSA is more likely to be taken up by B lymphoma cell lines than RAW264.7, thereby forming specific targeting of $CD22^{+}$ cells.

To further demonstrate the cell selectivity of F@TPSA, the uptake levels of Cy5@F@TPSA and Cy5@F@PLGA in RAW264.7 cells was compared (Fig. 7C and Figure S6). Obviously, there was no difference in the uptake of Cy5@F@TPSA and Cy5@F@PLGA by RAW264.7 cells, which ruled out the possibility that CD22-negative cells

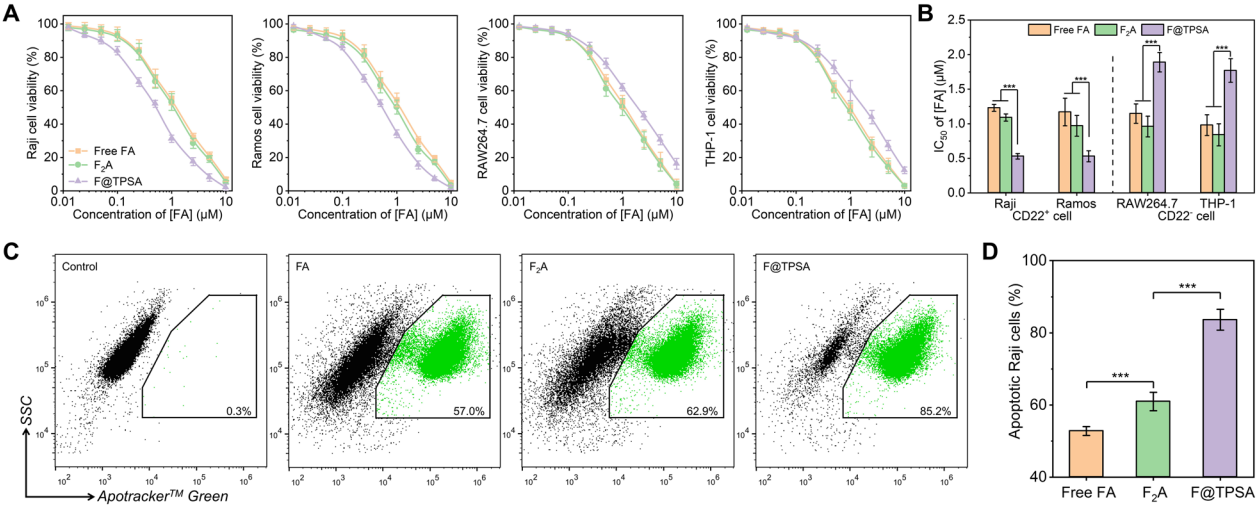

Fig. 8 In vitro anti-tumor effects of Free FA, F_2A, and F@TPSA in different cell lines. **A** Cytotoxicity of three FA formulations (Free FA, F_2A, and F@TPSA) against CD22-positive B lymphoma cell lines (Raji cells, Ramos cells) or CD22-negative other lymphocyte lines (RAW264.7 cells, THP-1 cells) was measured by MTT assay. **B** The half inhibitory concentrations (IC_{50}) of the three FA formulations on the above cells were compared. **C**, **D** Representative flow cytometry plots (**C**) and data statistics (**D**) of Raji cells treated for 1 h with three different FA formulations (all calculated as 1 μM FA). All data are presented the mean ± SD (n = 6). ***p < 0.001

had an uptake preference for F@TPSA. Remarkably, the uptake of Cy5@F@TPSA by Raji cells was about 2.3 times that of Cy5@F@PLGA (Fig. 7D, E). Dramatically, the uptake of Cy5@F@TPSA by Raji cells was significantly inhibited after pre-incubation of CD22-neutralizing antibody (αCD22). This further confirms that the specific targeting of F@TPSA to B lymphoma cell lines is mediated by CD22, which is also consistent with previous reports [29]. Furthermore, from Fig. 7F, G, it can be observed that under the same incubation time condition, Cy5 fluorescence intensity in Raji cells gradually increases with the increase of F@TPSA concentration, indicating that CD22-mediated endocytosis is concentration-dependent.

In vitro tumor inhibition effects of F@TPSA in different cell lines

After demonstrating the significant advantage of F@TPSA in specifically targeting CD22 positive B lymphoma cells, it is reasonable to speculate that F@TPSA has stronger cytotoxicity towards the aforementioned cells. The MTT method can be used to test the effects of different concentrations of FA preparations on the cell viability of four types of cells (including B lymphoma cells and other cells). As shown in Fig. 8A, as the concentration increases, all cell viability exhibits a non-linear decline. The apoptosis rates of Raji, Ramos, RAW264.7 and THP-1 cells were all over 80% at high concentrations (10 μM FA), regardless of FA, F_2A or F@TPSA. However, below 10 μM concentration, F@TPSA had a stronger negative effect on the viability of Raji and Ramos cells than FA and F_2A. Accordingly, it can also be seen from Fig. 8B that the IC_{50} of FA and F_2A in Raji cells are 1.2 ± 0.1 μM and 1.1 ± 0.1 μM, respectively. Surprisingly, the IC_{50} for F@TPSA is significantly reduced to 0.5 ± 0.1 μM. Similarly, when the IC_{50} of FA or F_2A to Ramos cells is 1.2 ± 0.2 μM and 1.0 ± 0.2 μM, respectively, Ramos cells also exhibit a more sensitive state to F@TPSA (the IC_{50} is 0.5 ± 0.1 μM). More interestingly, F@TPSA showed higher IC_{50} than FA and F_2A in two types of CD22 negative cells (RAW264.7 cells and THP-1 cells). It may be due to the lack of CD22 expression in RAW264.7 cells and THP-1 cells, resulting in weak uptake of F@TPSA, or due to low ROS levels in non B lymphoma cells, making it difficult to release FA encapsulated by TPSA. This also proves from another perspective that F@TPSA, a supramolecular nanoprodrug, not only enhances the cytotoxicity of FA to B lymphoma cell lines, but also enhances the tolerance of FA to other CD22-negative cells.

In addition, the apoptosis effects of three FA preparations (FA, F2A, F@TPSA) on Raji cells were further observed by flow cytometry (Fig. 8C). Apotracker™ Green, as a fluorescent probe, can label apoptotic cells by detecting phosphatidylserine residues located outside the cell membrane. As can be seen from Fig. 8D, although FA and F_2A (1.5 μM [FA]) could induce 52.8 ± 1.2% and 61.0 ± 2.6% apoptosis of Raji cells, respectively, F@TPSA caused led to more Raji cell apoptosis (83.7 ± 2.9%) under the same concentration. It is worth noting that TPSA has no effect on the cell viability of Raji cells up to 100 μM

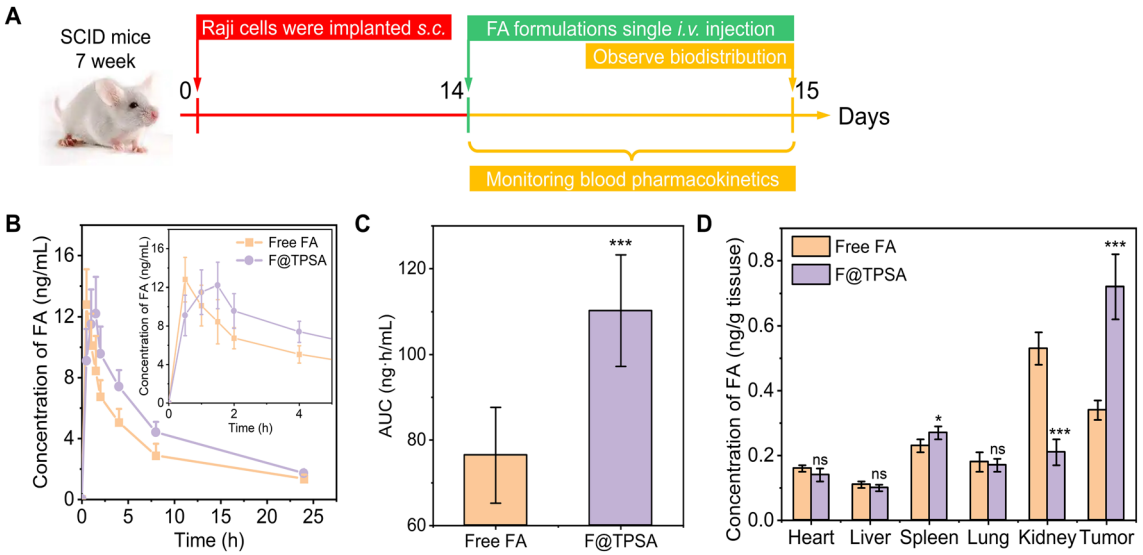

Fig. 9 Pharmacokinetics and biodistribution studies. **A** Protocol for B-NHL (Raji cell) xenograft model and monitor process. **B** The drug concentration of different FA formulations in the plasma of B-NHL xenograft mice model. **C** Cumulative amount of FA in plasma by calculating the area under the curve (AUC). **D** The FA content in major organs of tumor-bearing mice treated with FA or F@TPSA after 24 h. All data are presented the mean ± SD (n = 6). *p < 0.05, ***p < 0.001

(Figure S7). Therefore, the stronger apoptotic efficiency exhibited by F@TPSA can be attributed to the more precise delivery of FA by TPSA.

Pharmacokinetics and biodistribution of F@TPSA in B-NHL mouse model

Existing fludarabine injectable formulations have short half-lives, resulting in low bioavailability of FA. At the same time, in view of the wide distribution of lymphoid tissue, the clinical application of FA is mostly systematic administration, but the lack of FA targeting is easy to cause systemic toxicity. Therefore, innovative formulations play a crucial role in improving the aforementioned issues of FA.

The in vitro cell uptake experiments and cytotoxicity experiments have proved that F@TPSA can effectively achieve specific targeting and effective killing of CD22-positive B lymphoma cells, and it is reasonable to expect that F@TPSA can have good application in animal models. Therefore, B-NHL mouse model based on Raji cells was established, and the pharmacokinetic characteristics and biological distribution of supramolecular nanoprodrug F@TPSA in tumor-bearing mice were first investigated. Briefly, Raji cells were inoculated subcutaneously in SCID mice to establish a B-NHL model (Fig. 9A). When the tumor volume reaches 100 mm^3 (approximately 14 days), a single intravenous dose of free FA or F@TPSA (both at 100 mg/kg FA) is administered. The concentration of the FA in the blood is monitored at a predetermined time point. After 24 h, major organs of mice were collected for drug concentration detection.

Figure 9B shows the curve of drug concentration in the blood of tumor bearing mice over time. It can be seen that the FA concentrations in plasma of both Free FA and F@TPSA group presented a rapid increase, followed by a decreasing trend, which is consistent with the common phenomenon of intravenous injection. We know that nanoparticles are easily captured and eliminated by the reticuloendothelial system in vivo, but it is worth mentioning that the first half-life of F@TPSA (about 5.7 h) is longer than that of Free FA (about 2.5 h). This is also consistent with previous reports that endogenous PSA has immune escape and long circulation characteristics. In addition, although there was no significant difference in the maximum blood drug concentration (C_{max}) between Free FA and F@TPSA, the Free FA group mice reached their C_{max} at 0.5 h, while the F@TPSA group was delayed to around 1.5 h. This means that F@TPSA can reduce the sudden release of drugs in the body, thereby avoiding some of the side effects. It was precisely due to these differences in pharmacokinetic parameters that the area under the drug-time curve (AUC) of F@TPSA was about 1.44 times that of the Free FA group, reflecting a significant difference in the accumulation of drugs in the circulation system (Fig. 9C).

Furthermore, except pharmacokinetics, the distribution of F@TPSA in major organs (except heart, liver, and lung) was also different from that of Free FA (Fig. 9D). Most excitingly, 24 h after injection of F@TPSA, the

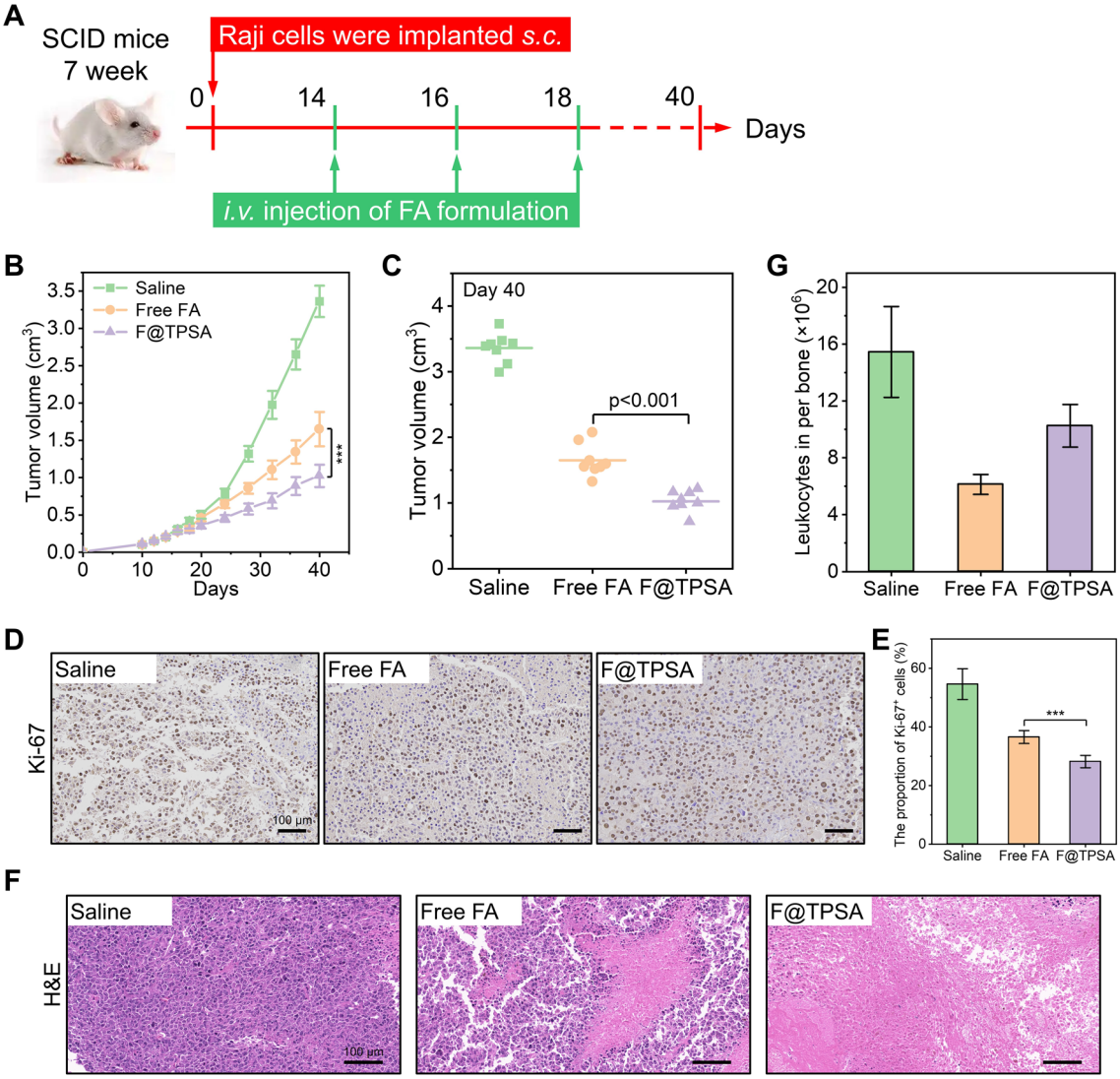

Fig. 10 The inhibitory effect of F@TPSA on the B-NHL xenograft mice model. **A** Establishment of B-NHL xenograft mice model and treatment regimen. At a dose of 100 mg/kg FA. **B** Tumor growth curves after various treatment. **C** On the 40th day, the tumor-bearing mice were sacrificed, tumor tissue were removed, and their volume was measured and calculated. **D**, **E** Representative microscopic images of Ki-67 immunohistochemical staining in tumor tissue sections (**D**) and proportion of Ki-67 positive cells (**E**). **F** Representative optical microscope image of H&E staining of tumor tissue sections. **G**, Leukocytes in a femur were collected and counted at 40th day. All data are presented the mean ± SD (n = 6). ***p < 0.001

amount of the drug in the tumor tissue was 2.1 times higher than in the Free FA group. This is also consistent with the trend of results in vitro cell experiments (Fig. 7), indicating that F@TPSA has the ability to target B-NHL in vivo. On the contrary, FA is thought to be excreted in urine and has certain nephrotoxicity. Therefore, the drug content in the kidneys of mice in the Free FA group was higher than that of F@TPSA, suggesting that F@TPSA would be less nephrotoxic. In addition, it is worth noting that drug concentration in the spleen of the F@TPSA group was about 17% higher than that of the Free FA group. This may be due to the fact that the spleen, as the largest lymphoid organ (55%–60% of lymphocytes are B cells), has a certain specific absorption of F@TPSA, suggesting that we should pay attention to the off-target effects of F@TPSA on the spleen.

Evaluation of antitumor effect and leukopenia of F@TPSA in vivo

These results prove that F@TPSA has a significant features of prolonged circulation time and excellent tumor

targeting ability in B-NHL mouse model constructed with Raji cells, which provides the basis for the accurate and efficient treatment of F@TPSA for this disease. Therefore, the same B-NHL mouse model was established and the curative effect of F@TPSA was observed. Briefly, tumor tissue volume was measured and calculated at a predetermined time point after receiving 3 injections of Free FA or F@TPSA (Fig. 10A). On the 40th day, tumor tissues of sacrificed mice were collected and sliced for observation by HE and Ki-67 staining.

The Fig. 10B shows the changes in tumor volume of tumor-bearing mice within 40 days. Obviously, the tumor volume of the three groups showed a significant difference in growth rate after the 20th day. The growth rate of saline group was the highest, while both Free FA and F@TPSA could inhibit the increase of tumor volume, while F@TPSA had a stronger inhibitory effect. Specifically, from Fig. 10C, by the 40th day, the tumor volume of saline group mice was 3.4 ± 0.2 cm^3, while the Free FA group and F@TPSA group were 1.7 ± 0.2 and 1.0 ± 0.2 cm^3, respectively. There was a significant difference between F@TPSA and Free FA. We know that Ki-67 is an antigen of proliferating cells, and its expression is positively correlated with the proliferation of tumor cells. The Ki-67 immunohistochemical staining photos of tumor tissue slices in Fig. 10D also show that the staining degree (brown) of the saline group is stronger than that of Free Fa and F@TPSA. After the statistics of Image-Pro Plus® software, the proportion of Ki-67 positive cells in the tumor tissues of mice in the Free FA group and the F@TPSA group was $36.6 \pm 2.2\%$ and $28.2 \pm 2.1\%$, which were both lower than $54.6 \pm 5.3\%$ in saline group (Fig. 10E). This proved that both Free FA and F@TPSA could inhibit the proliferation of tumor cells, but F@TPSA was more effective. Subsequently, H&E staining of tumor tissue sections also suggested that F@TPSA could cause a wider range of tumor tissue cell necrosis than Free FA (Fig. 10F). On the other hand, as a nucleoside drug, the most common side effect of FA is leukopenia, which is also an important factor limiting its clinical application. By counting total leukocytes in a single femur of tumor bearing mice (Fig. 10G), the leukocytes content in the saline treatment group mice is $15.5 \pm 3.2 \times 10^6$. However, Free FA significantly decreased leukocytes in tumor-bearing mice (only 39.6% of that in saline group), known as leukopenia. Encouragingly, there was only a 33.7% decrease in the F@TPSA group compared to the saline group. This reveals that F@TPSA can reduce the damage of FA to the hematopoietic system through better tumor targeting effect, and thus has better biocompatibility.

Conclusion

B-NHL is a hematological malignancy, but it cannot be treated with surgery due to its systemic distribution, so chemotherapy is still the first-line treatment. However, as a common clinical drug for B-NHL, the side effects caused by non-specific distribution of nucleoside antitumor drug fludarabine limit its long-term application. Drug delivery systems, especially targeted delivery systems, can significantly improve the aforementioned issues. Our preliminary research found that surface modification with PSA can assist in the enrichment of drug-loaded PLGA nanoparticles in the tumor site of B-cell lymphoma, indicating that PSA itself can also serve as a good B-NHL targeted carrier material. It is worth noting that compared to drug delivery systems based on physical encapsulation (represented by PLGA), prodrug based delivery systems have significant advantages in drug responsive release, drug loading, and reducing excipient usage. Therefore, in this study, we utilized the previously developed ROS responsive linker to prepare FA as a dimeric prodrug F_2A. At the same time, inspired by the Watson–Crick base pairing, thymine derivative (Thy-NH_2) was covalently grafted onto PSA to form a functional material TPSA. In aqueous solution, hydrogen bond is formed between adenine structure of F_2A and thymine structure of TPSA to induce cross-linking of TPSA material, and self-assembled supramolecular nanoprodrug F@TPSA is prepared. With the long circulation characteristics and specific targeting ability of endogenous PSA, F@TPSA can prolong the half-life of FA in tumor-bearing mice and achieve precise targeting of B-NHL, improve drug accumulation in tumor tissues, and achieve responsive drug release in tumor ROS microenvironment. Both in vitro cell experiments and in vivo experiments in mice, F@TPSA has achieved better anti-tumor effects than Free FA. More importantly, F@TPSA also reduces the accumulation of FA in the kidney and alleviates the myelosuppressive effect by enhancing the targeting effect. In summary, based on the tumor specific targeting performance derived from PSA and the supramolecular self-assembly inspired by "Watson–Crick" base pairing, this customized ROS activatable nanoprodrug has great potential in precise treatment of B-NHL.

Abbreviations

B-NHL	B-cell non-Hodgkin's lymphoma
FA	Fludarabine
ADC	Antibody–drug conjugations
CAR-T	Chimeric antigen receptor T-cell immunotherapy
PSA	Polysialic acid
PEG	Polyethylene glycol

PLGA	Poly(lactic-*co*-glycolic acid)
ICD	Immunogenic cell death
Thy-NH_2	3′-Amino-2′,3′-dideoxythymidine
TEM	Transmission electron microscope
DMEM	Dulbecco's Modified Eagle's medium
FBS	Fetal bovine serum
FITC	Fluorescein isothiocyanate
DCM	Dichloromethane
CDI	*N*,*N*′-Carbonyldiimidazole
HPLC	High performance liquid chromatography
NMR	Nuclear magnetic resonance
DLS	Dynamic light scattering
ESI–MS	Electrospray ionization mass spectrometry
A	Adenosine
T	Thymidine
MALDI-TOF MS	Matrix-assisted laser desorption ionization time-of-flight mass spectrometry
ROS	Reactive oxygen species
Cy5	Cyanine5

Supplementary Information

The online version contains supplementary material available at https://doi.org/10.1186/s12951-024-02745-5.

Supplementary Material 1.

Author contributions

Qixiong Zhang and Shanshan Li contribute the concepts of this work. Qixiong Zhang, Shanshan Li, Yuhan Tian, Yanrui Yang and Qiuying Huang completed the experimental study. Haibo Feng and Rui Zeng interpreted the data. Qixiong Zhang and Shanshan Li drafted and revised this paper. All authors reviewed the manuscript.

Funding

This work was supported by National Natural Science Foundation of China [82204304], Natural Science Foundation of Sichuan [2023NSFSC1678, 2024NSFTD0024, 2024NSFSC0197], Chengdu Science and Technology Program [2022YF05-01626-SN], Youth Innovation Project of Sichuan Medical Association [Q22006], Southwest Minzu University Research Startup Funds [RQD2022033], Open Project of Personalized Drug Therapy Key Laboratory of Sichuan Province [2022YB01], and the Scientific and Technological Innovation Team for Qinghai-Tibetan Plateau Research in Southwest Minzu University [2024CXTD15].

Availability of data and materials

No datasets were generated or analysed during the current study.

Declarations

Ethics approval and consent to participate

This work was approved by the ethics committee of Sichuan Academy of Medical Science & Sichuan Provincial People's Hospital.

Consent for publication

All authors read and agree this version be published.

Competing interests

The authors declare no competing interests.

Author details

[1]Department of Pharmacy, Personalized Drug Therapy Key Laboratory of Sichuan Province, Sichuan Academy of Medical Science & Sichuan Provincial People's Hospital, School of Medicine, University of Electronic Science and Technology of China, Chengdu 610072, China. [2]College of Pharmacy, Key Laboratory of Research and Application of Ethnic Medicine Processing and Preparation on the Qinghai-Tibet Plateau, Southwest Minzu University, Chengdu 610041, China. [3]College of Animal & Veterinary Sciences, Southwest Minzu University, Chengdu 610041, China.

Received: 19 May 2024 Accepted: 2 August 2024
Published online: 10 August 2024

References

1. Kuppers R. Mechanisms of B-cell lymphoma pathogenesis. Nat Rev Cancer. 2005;5:251–62.
2. Makita S, Tobinai K. Antibody therapy targeting CD19 for B-cell non-Hodgkin's lymphoma. Ann Oncol. 2018;29:1086–9.
3. Liu X, Zhao J, Guo X, Song Y. CD20 x CD3 bispecific antibodies for lymphoma therapy: latest updates from ASCO 2023 annual meeting. J Hematol Oncol. 2023;16:90.
4. Chinn P, Braslawsky G, White C, Hanna N. Antibody therapy of non-Hodgkin's B-cell lymphoma. Cancer Immunol Immunother. 2003;52:257–80.
5. Tan D, Tan SY, Lim ST, Kim SJ, Kim WS, Advani R, Kwong YL. Management of B-cell non-Hodgkin lymphoma in Asia: resource-stratified guidelines. Lancet Oncol. 2013;14:e548-561.
6. Lukenbill J, Kalaycio M. Fludarabine: a review of the clear benefits and potential harms. Leuk Res. 2013;37:986–94.
7. Gandhi V, Huang P, Plunkett W. Fludarabine inhibits DNA replication: a rationale for its use in the treatment of acute leukemias. Leuk Lymphoma. 1994;14(Suppl 2):3–9.
8. Hillmen P, Pitchford A, Bloor A, Broom A, Young M, Kennedy B, Walewska R, Furtado M, Preston G, Neilson JR, et al. Ibrutinib and rituximab versus fludarabine, cyclophosphamide, and rituximab for patients with previously untreated chronic lymphocytic leukaemia (FLAIR): interim analysis of a multicentre, open-label, randomised, phase 3 trial. Lancet Oncol. 2023;24:535–52.
9. Mehdizadeh M, Parkhideh S, Salari S, Hajifathali A, Rezvani H, Mabani M. Adverse effects of busulfan plus cyclophosphamide versus busulfan plus fludarabine as conditioning regimens for allogeneic bone marrow transplantation. Asian Pac J Cancer Prev. 2021;22:1639–44.
10. Mittal NK, Bhattacharjee H, Mandal B, Balabathula P, Thoma LA, Wood GC. Targeted liposomal drug delivery systems for the treatment of B cell malignancies. J Drug Target. 2014;22:372–86.
11. Jiang Y, Lin W, Zhu L. Targeted drug delivery for the treatment of blood cancers. Molecules. 2022;27:1310.
12. Liu Y, Zhou X, Wang X. Targeting the tumor microenvironment in B-cell lymphoma: challenges and opportunities. J Hematol Oncol. 2021;14:125.
13. Duan S, Paulson JC. Siglecs as immune cell checkpoints in disease. Annu Rev Immunol. 2020;38:365–95.
14. Xu J, Luo W, Li C, Mei H. Targeting CD22 for B-cell hematologic malignancies. Exp Hematol Oncol. 2023;12:90.
15. Mullard A. Maturing antibody-drug conjugate pipeline hits 30. Nat Rev Drug Discov. 2013;12:329–32.
16. Stokke JL, Bhojwani D. Antibody-drug conjugates for the treatment of acute pediatric leukemia. J Clin Med. 2021;10:3556.
17. Fry TJ, Shah NN, Orentas RJ, Stetler-Stevenson M, Yuan CM, Ramakrishna S, Wolters P, Martin S, Delbrook C, Yates B, et al. CD22-targeted CAR T cells induce remission in B-ALL that is naive or resistant to CD19-targeted CAR immunotherapy. Nat Med. 2018;24:20–8.
18. Ramakrishna S, Highfill SL, Walsh Z, Nguyen SM, Lei H, Shern JF, Qin H, Kraft IL, Stetler-Stevenson M, Yuan CM, et al. Modulation of target antigen density improves CAR T-cell functionality and persistence. Clin Cancer Res. 2019;25:5329–41.
19. Mindler K, Ostertag E, Stehle T. The polyfunctional polysialic acid: a structural view. Carbohydr Res. 2021;507: 108376.
20. Shi Y, Lu A, Wang X, Belhadj Z, Wang J, Zhang Q. A review of existing strategies for designing long-acting parenteral formulations: focus on underlying mechanisms, and future perspectives. Acta Pharm Sin B. 2021;11:2396–415.
21. Fernandes AI, Gregoriadis G. Synthesis, characterization and properties of sialylated catalase. Biochim Biophys Acta. 1996;1293:90–6.
22. Fernandes AI, Gregoriadis G. The effect of polysialylation on the immunogenicity and antigenicity of asparaginase: implication in its pharmacokinetics. Int J Pharm. 2001;217:215–24.
23. Kou Y, Feng R, Chen J, Duan L, Wang S, Hu Y, Zhang N, Wang T, Deng Y, Song Y. Development of a nattokinase-polysialic acid complex for advanced tumor treatment. Eur J Pharm Sci. 2020;145: 105241.

24. Jain S, Hreczuk-Hirst DH, McCormack B, Mital M, Epenetos A, Laing P, Gregoriadis G. Polysialylated insulin: synthesis, characterization and biological activity in vivo. Biochim Biophys Acta. 2003;1622:42–9.
25. Wu JR, Lin Y, Zheng ZY, Lin CC, Zhan XB, Shen YQ. Improvement of the CuZn-superoxide dismutase enzyme activity and stability as a therapeutic agent by modification with polysialic acids. Biotechnol Lett. 2010;32:1939–45.
26. Tiede A, Allen G, Bauer A, Chowdary P, Collins P, Goldstein B, Jiang HJ, Köck K, Takacs I, Timofeeva M, et al. SHP656, a polysialylated recombinant factor VIII (PSA-rFVIII): First-in-human study evaluating safety, tolerability and pharmacokinetics in patients with severe haemophilia A. Haemophilia. 2020;26:47–55.
27. Kelm S, Gerlach J, Brossmer R, Danzer CP, Nitschke L. The ligand-binding domain of CD22 is needed for inhibition of the B cell receptor signal, as demonstrated by a novel human CD22-specific inhibitor compound. J Exp Med. 2002;195:1207–13.
28. Hong S, Yu C, Wang P, Shi Y, Cao W, Cheng B, Chapla DG, Ma Y, Li J, Rodrigues E, et al. Glycoengineering of NK cells with glycan ligands of CD22 and selectins for B-cell lymphoma therapy. Angew Chem Int Ed Engl. 2021;60:3603–10.
29. Zhang Q, Li S, Guo K, Yin X, Tong R. Polysialylated nanoinducer for precisely enhancing apoptosis and anti-tumor immune response in B-cell lymphoma. Acta Biomater. 2022;149:321–33.
30. Li S, Shan X, Wang Y, Chen Q, Sun J, He Z, Sun B, Luo C. Dimeric prodrug-based nanomedicines for cancer therapy. J Control Release. 2020;326:510–22.
31. Zhang Q, Li S, Bai L, Yu D, Li H, Tong R. Self-delivery janus-prodrug for precise immuno-chemotherapy of colitis-associated colorectal cancer. ACS Appl Mater Interfaces. 2022;14:297–306.
32. Zhang Q, Li S, Ren J, He X, Shi H, Zhang F, Li H, Tong R. ROS-triggered nanoinducer based on dermatan sulfate enhances immunogenic cell death in melanoma. J Control Release. 2022;348:22–33.
33. Li S, Xie A, Li H, Zou X, Zhang Q. A self-assembled, ROS-responsive Janus-prodrug for targeted therapy of inflammatory bowel disease. J Control Release. 2019;316:66–78.

Publisher's Note